Fabrication of polyaniline (PANI) through parallel nanopores; transport properties of PANI@SiO2 nanopore molecular junctions

Xiaonan Sun, Wahid Ullah, Jean-Christophe Lacroix, Alain Walcarius, Grégoire Herzog, Neus Vilà

Fabrication of polyaniline (PANI) through parallel nanopores; transport properties of PANI@SiO_2 nanopore molecular junctions

Xiaonan Sun[a*], Wahid Ullah[b], Jean-Christophe Lacroix[a], Alain Walcarius[b], Grégoire Herzog[b], Neus Vilà[b*]

[a]*Université Paris Cité, CNRS, ITODYS, F-75013 Paris, France*

[b]*Université de Lorraine, CNRS, LCPME UMR 7564, Nancy, France*

e-mail: neus.vila@univ-lorraine.fr, sun.xiaonan@univ-paris-diderot.fr

Abstract

Aniline is electropolymerized through mesoporous silica nanopores (100 nm-long, 3 nm in diameter) orthogonally oriented on indium-tin oxide (ITO). Only a few polyaniline (PANI) wires are accommodated in the nanochannels and their growth is electrochemically controlled. The electronic transport properties of PANI@SiO_2 are studied by Conductive Atomic Force Microscopy (C-AFM), using a Pt-coated C-AFM tip as a top electrode to complete ITO/PANI@SiO_2/Pt molecular junctions (MJs). Three different behaviors are observed. First, linear I/V curves are obtained when PANI is deposited in the nanopores with material spilling over the silica membrane. Transport occurs through many PANI@SiO_2 channels where the overall conductance is high. Second, flat I/V curves are recorded, indicating "insulator" behavior when the SiO_2 nanopores are not fully filled by PANI wires. Thirdly, non-linear I/V curves, which are quantitatively highly reproducible and independent of the area probed, are obtained. These are attributed to the formation of MJs where the C-AFM tip in contact with nanopores acts as the top electrode with vertical PANI wires just filling the SiO_2 channels.

Introduction

The sol-gel process emerges as a strategy to obtain organic-inorganic nanocomposites in which mesoporous silica matrices serve as hosts/templates for the confinement of various types of functional molecules. Such nanocomposite materials combine the properties of guest molecules with the attractive features of mesoporous silica (high stability, transparency, convenient processing and shaping). They offer considerable interest for potential applications in the next generation of molecular-based devices, including plasmonic waveguides, photonic crystals, memory storage devices, or photovoltaics. [1-6] The easy processability of silica sol-gels, especially to form organic-inorganic hybrid materials, is also

very appealing for optics, molecular electronics, catalysis or electrocatalysis. [7-11] Mesoporous materials can be manufactured in several morphologies, but the insertion of organic molecules/polymers, undoubtedly offers many advantages in view of novel devices for target applications. [12] The control over the orientation of the mesopores on a macroscopic scale is a further advantage of these materials, as it allows the placement of guest molecules in well-defined positions and the thorough determination of molecular events in the channels. [13] Ordered mesoporous silica thin films are usually prepared by evaporation-induced self-assembly, [10,12,14] but getting mesopore channels oriented orthogonally to the underlying support has required the development of more specific methods. [15-17] Among them, electrochemically assisted self-assembly (EASA) has proven to be a simple, versatile, and fast way to generate vertically aligned mesoporous silica membranes on electrode surfaces. [15,18] The vertically oriented and hexagonally packed mesochannels of electrogenerated silica films offer an ideal configuration for applications in the sensor field. [17-20] However, fast diffusion processes and high sensitivity, associated with their vertical alignment, [21,22] have not yet been exploited in molecular electronics.

Embedding conductive polymers into mesoporous hosts opens up the possibility of complementing their molecular redox and optical properties with the chemical and mechanical stability of the host. Some examples exist of the use of nanoporous membranes for growing polythiophene [23], polypyrrole [24], PANI [25], and other conductive polymers. [26,27] The nanowires obtained exhibit, most often, diameters larger than the pore size of the nanoporous matrix. We have previously described the growth by electropolymerization of ultra-thin nanoarrays of PANI filaments covalently bonded to underlying ITO electrodes modified with vertically oriented silica films. Molecular junctions (MJs) based on self-assembled monolayers (SAMs) have been described using conductive polymers as contacts to eliminate shorts through the SAMs. [28] In this paper, we describe for the first time the electrical properties of PANI filaments grown in a nanoporous non-conductive vertically oriented silica matrix. The scientific questions are: (i) can we grow PANI nanowires inside 3 nm-diameter nanopores of a mesoporous insulating silica host and control this growth so that the wires have the same length as the nanopores? (ii) can we study by C-AFM the transport properties of a few conductive PANI wires confined inside the nanopores?

Experimental Section

Chemicals and reagents

Tetraethoxysilane (TEOS, 98%, Sigma Aldrich), ethanol (95–96% Merck), $NaNO_3$ (99%, Fluka), HCl (Riedel de Haan, 1 M solution), trimethyloctadecyltrimethylammonium bromide (ODAB; 98% Sigma Aldrich) were used as received for mesoporous silica film electrosynthesis. Reagents for electrografting were purchased from Sigma Aldrich and used as received: p-phenylenediamine (98%), $NaNO_2$ (97%).

Aniline (99.5%, Sigma Aldrich) was distilled under vacuum before use. H_2SO_4 (98%, Sigma) was used as the electrolyte for the electrochemical characterization of PANI. NaOH (VWR International) was used to dissolve the silica template.

Generation of PANI nanofilaments.

To an aqueous solution containing 5 mM *p*-phenylenediamine was added 5 mM $NaNO_2$ in 0.5 M HCl. The mixture was allowed to react for 10 min under stirring at room temperature, leading to the formation of aminophenyl monodiazonium cations. This solution of *in situ*-generated species was used for their electrochemical reduction at -0.2 V for 1 min on ITO electrodes covered with vertically aligned mesoporous silica films (which were prepared as previously described [15,21]) in order to covalently attach aminophenyl groups to the ITO surfaces located at the bottom of the mesochannels (the area covered with PANI was 0.125 cm^2). The modified ITO substrates were then thoroughly rinsed with water and sonicated for 5 min in ethanol to remove unreacted diazonium species. PANI nanofilaments were then electrochemically generated from a solution of 0.1 M aniline (in 0.5 M H_2SO_4) at +0.85 V under potentiostatic conditions. The same experiments were carried out with bare ITO electrodes for comparison purposes. Template-free PANI nanofilaments were obtained by chemical etching of the mesoporous silica films by soaking them in a 1 M NaOH solution for 10 min.

Apparatus and procedures for material characterization.

All electrochemical experiments were performed with a PGSTAT 100 or a μAutolab from Ecochemie (Metrohm) operated by NOVA software (Autolab). Two three-electrode electrochemical cells were used: a first homemade one for film synthesis using an ITO plate as working electrode, a silver rod pseudo-reference electrode and a stainless-steel counter-electrode; a second homemade one for electrografting, electropolymerization and cyclic voltammetry characterization using the ITO plates after deposition of the silica films as working electrodes, an Ag/AgCl 1 M KCl reference electrode (Metrohm) and a platinum wire counter-electrode. The mesoporous films were observed by transmission electron microscopy (TEM) using a JEOL ARM200F (after mechanically removing portions of the film from the ITO surface). The film mesostructure was also analyzed by grazing-incidence small-angle X-ray scattering (GISAXS). Conductive Atomic Force microscopy (C-AFM) from Resiscope II SCIENTEC, with Pt-coated C-AFM probes, was used to characterize the electronic property of the well-defined PANI-filled mesoporous films.

Results and discussion

Polyaniline (PANI) nanowires were generated by potentiostatic electropolymerization through an oriented mesoporous silica film previously formed by electrochemically assisted self-assembly (EASA) on an ITO electrode [13,15]. The ITO surface at the bottom of the nanochannels was first derivatized with aniline moieties to ensure covalent bonding with the PANI nanowires; this was achieved according

to a previously reported procedure involving the electrochemical reduction of *in situ*-generated aminophenyl monodiazonium salt (electrografting) [21]. This procedure, generating an ultrathin layer of π-conjugated oligomers covalently grafted to the electrode, has been widely used to improve the adhesion of conductive polymers to various substrates. [30-32] Figure 1A shows the typical I-t curve recorded during the electropolymerization of aniline through the mesoporous membrane at +0.85 V. This curve is characterized by three domains: a first nucleation step leading to the formation of oligomers, then a rate-determined growth of PANI wires through the nanochannels, and finally a subsequent fast 3-dimensional growth of bulk PANI outside the membrane (see the corresponding schemes in Figure 1A). Thanks to the very regular hexagonal packing of vertically aligned 3 nm-diameter mesochannels (Figure $1B_1$), one can get a very high density of PANI nanowires physically isolated from each other and tune their length by appropriate adjustment of the electropolymerization time. Up to 120 s, PANI wires are only present in the nanochannels and the membrane surface appears smooth (Figure $1B_2$), whereas longer electropolymerization times lead to the formation of bulk PANI deposits on top of the silica membrane (Figure $1B_3$). The presence of PANI can be indirectly proven by the detection of nitrogen species in energy-dispersive analysis of X-rays associated to transmission electron microscopy [29]). Moreover, the existence of PANI in the emeraldine form is clearly demonstrated by UV-visible spectroscopy which shows an absorption band at λ = 720-750 nm (corresponding to the polaron state of the green emeraldine salt) and the π-π* transition of the aromatic rings (at λ = 430-440 nm) (Figure 1C). The main band was stronger for PANI electrogenerated for longer times, as a result of larger amounts of polymer growing out of the silica membrane. Due to the larger tip diameter, individual PANI nanowires are difficult to visualize directly by AFM topography.

Figure 2A compares the cyclic voltammogram (CV) characteristics of PANI materials obtained by electropolymerization through the nanochannels for two distinct growth times (100 and 160 s). In both cases, they reveal the reversible transformation of the leucoemeraldine-emeraldine system [22,32,33], but show much larger currents for the sample with bulk PANI deposits over the silica membrane than for the sample with PANI nanowires located only in the mesochannels. This is, of course, due to larger amounts of PANI in the former case (as confirmed by a more intense green color, see insets in Figure 2A), but it may also indicate slower charge transfer processes for such small wires confined in the mesoporous membrane, due to diffusional restrictions during doping and dedoping. The PANI spills beyond the silica matrix and thus forms a layer on top of it. This provides useful information for the C-AFM characterization described below. Figure 2B depicts the CV curves for the same electrodes but as recorded at various potential scan rates. They indicate a thin-layer behavior (peak currents directly proportional to the potential scan rate), suggesting that electron transfer processes are likely to occur through the whole thickness of the insulating silica membrane. This observation thus makes the investigation of their conductance properties promising.

To investigate the transport properties of PANI@SiO_2 films, a conductive atomic force microscope (C-AFM) was used to directly map the resistive/conductive areas of an electrode. C-AFM measurements were performed under N_2 atmosphere at room temperature to avoid contamination. Pt-coated conductive C-AFM probes were put into soft contact with the films, with a controlled force of less than 5 nN so that the probes do not penetrate the film.

The PANI-filled nanoporous film is characterized by concurrent images of topography and current (Figure 3 a, b). The experimental set-up is schematically shown in Figure 3a, where the tip radius is less than 10 nm. The film shows nanoscale flatness and a roughness of less than 5 nm (Figure 3b) thanks to the high quality of the mesoporous silica films. The local electrical conductance of the films was first characterized by measuring, at constant bias, the current between the probe tip and the sample while scanning in the contact mode. Current mapping is shown in Figure 3c. When the applied voltage is less than 0.1 V, the films are uniformly insulating (current level of tens of pA). When a bias voltage of -2 V is applied, the current levels in the red and the blue zones are between 1 and 2 nA. Only the yellow zones are not conductive (Figure 3c). An important result is that the conductive areas of the films cover most of the C-AFM image, i.e. 1 μm^2.

Typical current vs. voltage (I/V) curves were recorded by sweeping the applied bias voltage range at various points on the PANI@SiO_2 film. Figure 4a shows combined I/V curves at different points of the PANI@SiO_2 film, displaying three typical text-book conductive/resistive behaviors. First, there are linear I/V plots where the current is directly proportional to the applied potential difference (in the voltage range investigated). The current seems to follow Ohm's law and to indicate metallic conductivity. This behavior appears when PANI is deposited both in the nanopores and over the silica membrane. In this situation, transport occurs through many parallel PANI@SiO_2 channels. The overall conductance and, therefore, the current are high, and the C-AFM amplifiers are saturated at low bias. Second, an almost flat I/V graph can be observed. They indicate an "insulator" behavior where zero current is recorded whatever the applied potential. This corresponds to the situation where the SiO_2 pores are not completely filled and the C-AFM probe is not in contact with any conductive PANI wires. The last and most frequent occurrence is that the I/V curves are non-linear, which are typical of MJs. [34-41] Several MJs I/V curves were recorded at different applied bias potential ranges (Figure 4b). When the same potential range is swept, the curves recorded at different points show very good reproducibility and can almost be overlaid. This indicates that the conductance is independent of the spot probed by the C-AFM tip and suggests that MJs are formed with well-defined size. This behavior is, therefore, attributed to the formation of MJs where the C-AFM probe is in contact with nanopores whose SiO_2 channels are just filled by the vertical PANI wires. Because of the nanoscale size of the C-AFM tip (tip radius < 10 nm), the radius of the top contact to these PANI-based MJs cannot exceed 5 nm. This suggests that the tip is seeing less than 5 nanopores each filled with one or two PANI wires.

Finally, all I/V curves show symmetric behavior, indicating no preferred current flow despite the use of two different electrodes and electrode/molecule electronic coupling at the bottom or top interface. Moreover, hysteresis-type of behavior is observed at room temperature, although the back/forth ratio is low. Figure 4b shows hysteresis-type I/V curves from −3 to 3 V and −5 to 5 V and in the reverse direction. The observation of the hysteresis loops is normally an indication of a MJ memory effect. With a sweep voltage of 5 V the current amplitude, as well as the back/forth current ratio (at an applied bias of 2 V, for example), is lower than those of the 3 V. Charge transport is thus dependent of the range of the sweeped voltage.

In summary, PANI nanowires have been electrodeposited through individual mesoporous silica nanopores orthogonally oriented on ITO electrodes. When the PANI wires completely fill individual nanopores, the electronic transport properties of the PANI@SIO_2 systems are such that I/V curves are non-linear and are quantitatively highly reproducible on several points of the film. This suggests that the C-AFM tip is seeing about 5 nanopores each filled with one or two PANI wires and that MJs consisting of few nanopores incorporating various types of electroactive or photoactive molecules could be easily generated in the same way**.**

Acknowledgments

The authors acknowledge the support of the French Agence Nationale de Recherche (ANR), under grant Project-ANR-20-CE09-0004. This work was also partly supported by the French PIA project "Lorraine Université d'Excellence" (Reference No. ANR-15-IDEX-04-LUE). WU acknowledges a PhD grant from Lorraine University. . Dr. John Lomas is warmly thanked for the English edition of the manuscript.

References:

1. Tahri, Z.; Lepski, R.; Hsieh, K.-Y.; Bendeif, E.-E.; Pillet, S.; Durand, P.; Woike T.; Schaniel, D. *Phys. Chem. Chem. Phys.* **2012**, *14* , 3775–3781.
2. Durand, P.; Pillet, S.; Bendeif, E.-E.; Carteret, C.; Bouazaoui, M.; Hamzaoui, H. E.; Capoen, B.; Salmon, L.; Hébert, S.; Ghanbaja, J.; Aranda, L.; Schaniel, D. *J. Mater. Chem. C* **2013**, *1*, 1933–1942.
3. (a) Ariga, K.; Vinu, A.; Hill, J. P.; Mori, T. *Coord. Chem. Rev.* **2007**, *251*, 2562–2591. (b) Moller, K.; Bein, T. *Chem. Mater.* **1998**, *10*, 2950–2963.
4. Sanchez, C.; Lebeau, B. *MRS Bull.* **2001**, *26*, 377–387.
5. Sanchez, C.; Lebeau, B.; Chaput, F.; Boilot, J.-P. *Adv. Mater.* **2003**, *15*, 1969–1994.
6. Wan, Y.; Zhao, D. *Chem. Rev.* **2007**, *107*, 2821–2860.
7. Vivero-Escoto, J.L.; Trewyn, B.G.; Lin, V.S-Y. *Annu. Rev. Nano Res.* **2010**, *3*, 191–231.
8. (a) Walcarius, A.; Mercier, L. *J. Mater. Chem.* **2010**, *20*, 4478-4511. (b) Vallet-Regi, M.; Colilla, M.; Gonzalez, B. *Chem. Soc. Rev.* **2011**, *40*, 596–607.
9. Lebold, T.; Michaelis, J.; Braeuchle, C. *Phys. Chem. Chem. Phys.* **2011**, *13*, 5017–5033.
10. Innocenzi, P.; Malfatti, L. *Chem. Soc. Rev.* **2013**, *42*, 4198–4216.
11. Cho, J.; Ishida, Y. *Adv. Mater.* **2017**, *29*, 1605974.
12. Grosso, D.; Cagnol, F.; Soler-Illia, G. J. d. A. A.; Crepaldi, E. L.; Amenitsch, H.; Brunet-Bruneau, A.; Bourgeois, A.; Sanchez, C. *Adv. Funct. Mater.* **2004**, *14*, 309–322.
13. Walcarius, A.; Sibottier, E.; Etienne, M.; Ghanbaja, J. *Nat. Mater.* **2007**, *6*, 602–608.
14. Etienne, M.; Walcarius A. *Electrochem. Commun.* **2005**, *7*, 1449–1456.

15. Goux, A.; Etienne, M.; Aubert, E.; Lecomte, C.; Ghanbaja, J.; Walcarius, A. *Chem. Mater.* **2009**, *21*, 731–741.
16. (a) Teng, Z.; Zheng, G.; Dou, Y.; Li, W.; Mou, C.-Y.; Zhang, X.; Asiri, A. M.; Zhao, D. *Angew. Chem. Int. Ed.* **2012**, *51*, 2173–2177. (b) Kao, K.-C.; Lin, C.-H.; Chen, T.-Y.; Liu, Y.-H.; Mou, C.-Y. *J. Am. Chem. Soc.* **2015**, *137*, 3779–3782.
17. Walcarius, A. *Electroanalysis* **2015**, *27*, 1303–1340.
18. Yan, F.; Lin, X.; Su, B. *Analyst* **2016**, *141*, 3482–3495.
19. Zhou, Z.; Guo, W.; Xu, L.; Yang, Q.; Su, B. *Anal. Chim. Acta* **2015**, *886*, 48–55.
20. Nasir, T.; Herzog, G.; Liu, L.; Hébrant, M.; Despas, C.; Walcarius, A. *ACS Sensors* **2018**, *3*, 484–493.
21. Ullah, W.; Herzog, G.; Vilà, N.; Walcarius, A. *Electrochem. Commun.* **2021**, *122*, 106896.
22. Walcarius, A. *Curr. Opin. Electrochem.* **2018**, *10*, 88–97.
23. del Valle, M.A.; Gacitúa, M.; Díaz, F.R.; Armijo, F.; del Río, R. *Electrochem. Commun*. **2009**, *11,* 2117–2120.
24. Kang, H.; Lee, H.; Kwak J. *J. Korean Electrochem. Soc*. **2011**, *14*, 22–26.
25. Ding, L,; Li, W.; Wang, Q.; Sun, Q.; He, Y.; Su. B. *Chem. Eur. J.* **2014**, *20*, 1829–1833.
26. del Valle, M.A.; Hernández, L.A.; Díaz, F.R.; Ramos. A. *Int. J. Electrochem. Sci.* **2015**, *10*, 5152–5163.
27. (a) Hernández, L.A., del Valle, M.A.; Díaz, F.R.; Fermín, D.J.; Risbridger. T.A.G. *Electrochim. Acta* **2015**, *166*, 163–167. (b)Vacca, A.; Mascia, M.; Rizzardini, S.; Palmas, S.; Mais, L. *Electrochim. Acta*, **2014**, *126,* 81–89.
28. Santos, L. M.; Ghilane, J.; Fave, C.; Lacaze, P.C.; Randriamahazaka, H.; Abrantes, L.M.; Lacroix, J. C. *J. Phys. Chem. C* **2008**, *112*, 16103–16109.
29. Gamero-Quijano, A.; Karman, C.; Vilà, N.; Herzog, G.; Walcarius, A. *Langmuir* **2017**, 33, 4224–4234.
30. Villemin, E.; Lemarque, B.; Vũ, T.T.; Nguyen, V.Q.; Trippé-Allard, G.; Martin, P.; Lacroix, J. C. *Synth. Met.* **2019**, *248*, 45–52.
31. Gam-Derouich, S.; Carbonnier, B.; Turmine, M.; Lang, P.; Jouini, M.; Ben Hassen-Chehimi, D.; M. Chehimi, M. *Langmuir* **2010**, *26*, 11830–11840.
32. Lacroix, J. C.; Kanazawa, K. K.; Diaz, A. *J. Electrochem. Soc.* **1989**, *136*, 1308–1313.
33. Janin, M.; Ghilane, J.; Lacroix, J. C. *J. Am. Chem. Soc.* **2013**, *135*, 2108–2111.
34. Han, Y.; Nickle, C.; Zhang, Z.; Astier, H. P.; Duffin, T. J.; Qi, D.; Wang, Z.; del Barco, E.; Thompson, D.; Nijhuis, C. A. *Nat. Mater.* **2020**, *19*, 843–848.
35. Chen, X.; Roemer, M.; Yuan, L.; Du, W.; Thompson, D.; del Barco, E.; Nijhuis, C. A. *Nat. Nanotechnol.* **2017**, *12*, 797–803.
36. Jiang, L.; Sangeeth, C. S.; Yuan, L.; Thompson, D.; Nijhuis, C. A. *Nano Lett.* **2015**, *15*, 6643–6649.
37. Ho Choi, S.; Kim, B.; Frisbie, C. D. *Science* **2008**, *320*, 1482–1486.
38. Luo, L.; Frisbie, C. D. *J. Am. Chem. Soc.* **2010**, *132*, 8854–8855.
39. Nguyen, Q. V.; Martin, P.; Frath, D.; Della Rocca, M. L.; Lafolet, F.; Bellinck, S.; Lafarge, P.; Lacroix, J. C. *J. Am. Chem. Soc.* **2018**, *140*, 10131–10134.
40. Tefashe, U. M.; Nguyen, Q. V.; Lafolet, F.; Lacroix, J. C.; McCreery, R. L. *J. Am. Chem. Soc.* **2017**, *139*, 7436–7439.
41. Lacroix, J. C. *Curr. Opin. Electrochem.* **2018**, *7*, 153–160.
42. Goswami, S., Matula, A. J., Rath, S. P., Hedström, S., Saha, S., Annamalai, M.; Sengupta, D.; Patra, A.; Ghosh, S.; Jani, H.; Sarkar, S.; Motapothula, M.R.; Nijhui, C.A.; Martin, J.; Goswami, S.; Batista, V.S.; Venkatesan, T. *Nat. Mater.* **2017**, *16*, 1216–1224.
43. Lin, Y. P.; Bennett, C. H.; Cabaret, T.; Vodenicarevic, D.; Chabi, D.; Querlioz, D.; Jousselme, B.; Derycke, V.; Klein, J. O. *Sci. Rep.* **2016**, *6*, 31932.

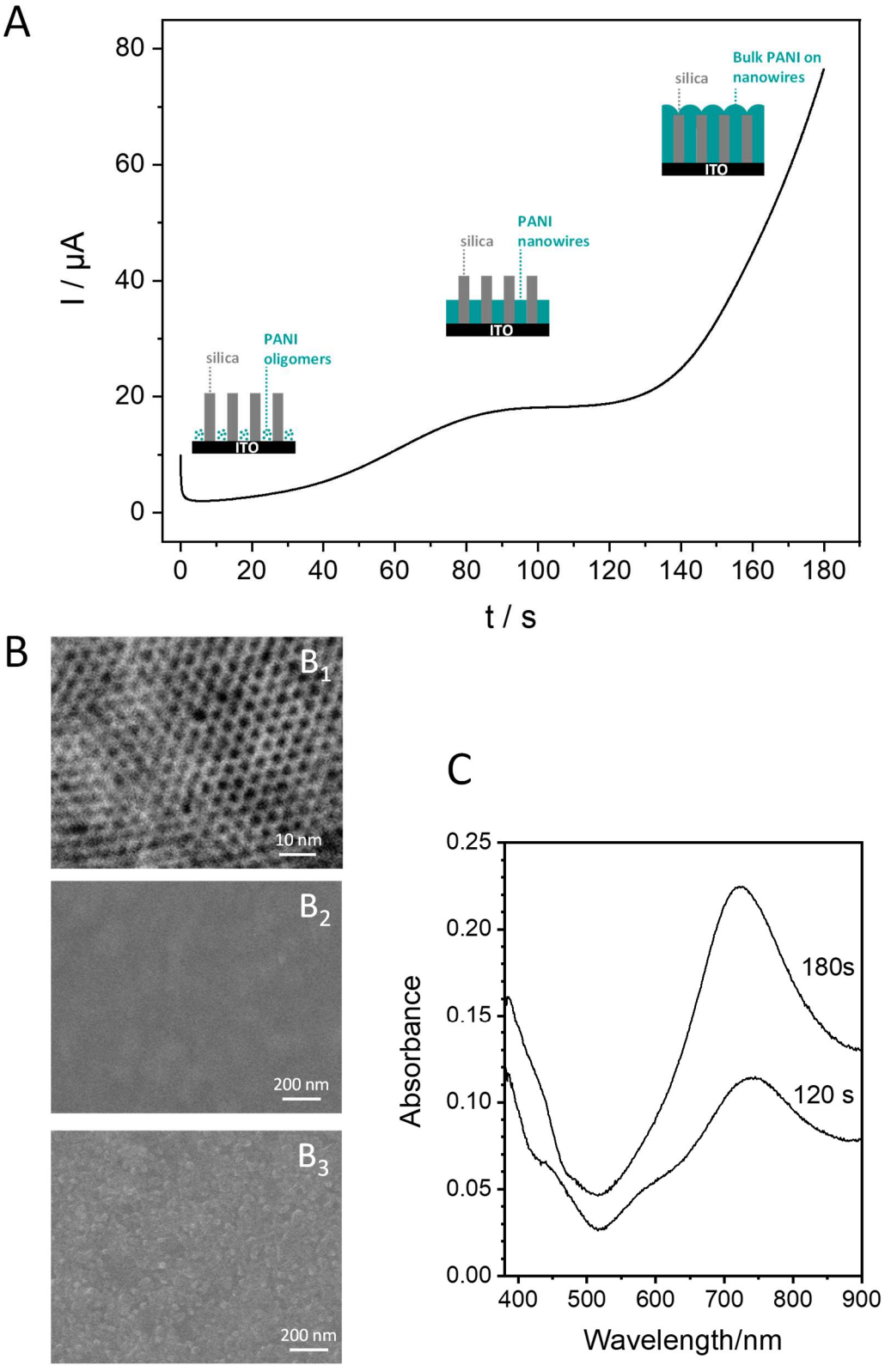

Figure 1. (A) I – t curves recorded during PANI electropolymerization in 0.1 M aniline (in 0.5 M H_2SO_4) at constant potential (+0.85 V) using an ITO electrode covered with vertically oriented mesoporous silica film, which was previously electrografted with aminophenyl groups (the three steps of the electropolymerization process are illustrated) The electropolymerization of PANI was carried out on an area of 0.125 cm^2. (B) Electron microscopy imaging of the film surface: (B_1) STEM top view of the highly ordered mesopore channels; (B_2 & B_3) SEM top views of the mesoporous film after PANI growth for 100 s (B_2) and 160 s (B_3), respectively. (C) UV-vis spectra

of the oxidized form of PANI nanowires generated through mesoporous silica films for two electropolymerization times (120 s or 180 s; see indication on plots).

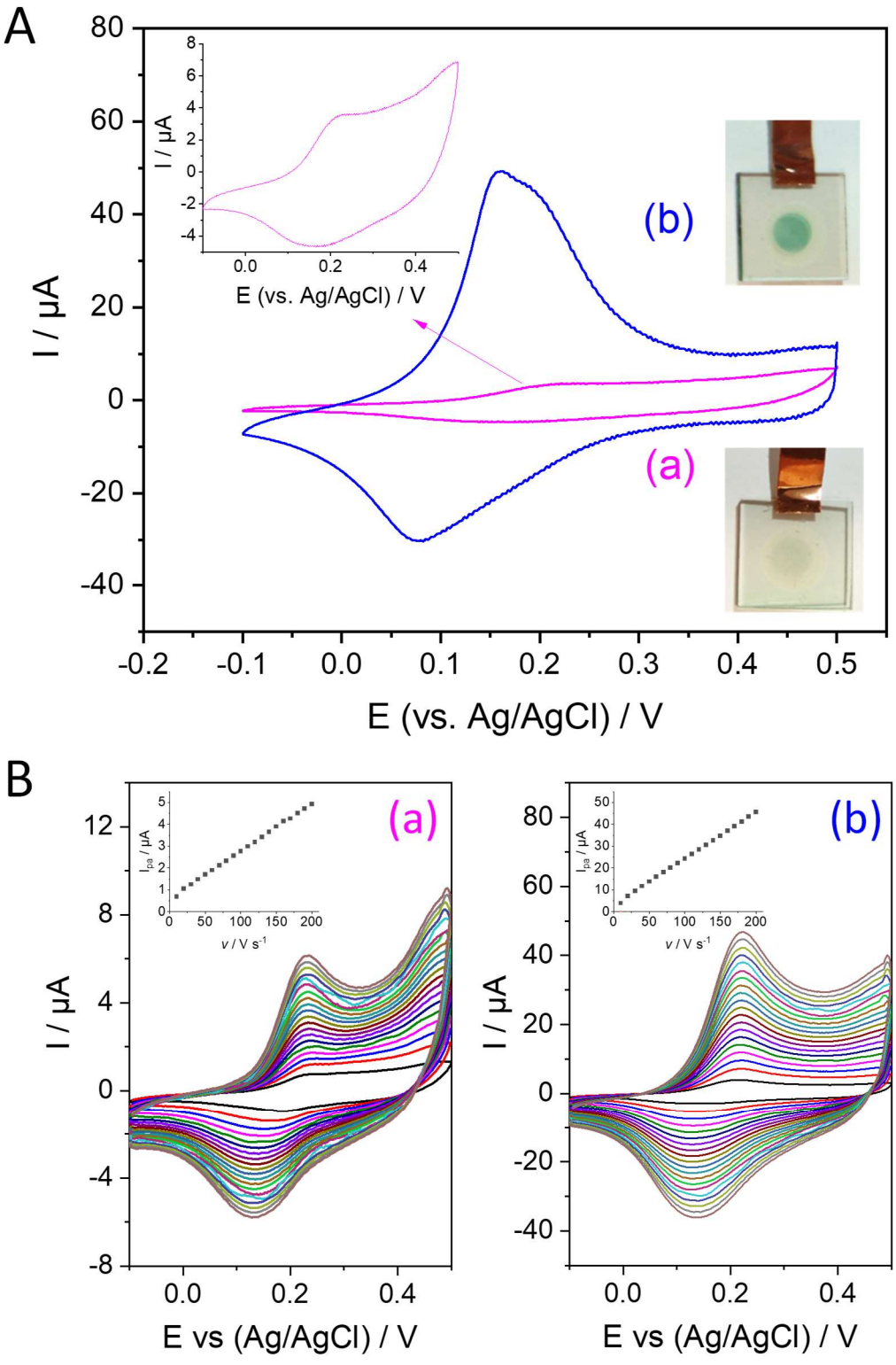

Figure 2. Cyclic voltammetry characterization of PANI nanowires generated through mesoporous silica film for electropolymerization times of (a) 100 s and (b) 160 s; (A) CV curves recorded at 50 mV s^{-1} in 0.5 M H_2SO_4 (left inset represents an enlargement of curve (a) while right insets portray the ITO/mesoporous silica film electrodes obtained after electropolymerization in both cases); (B) CV curves recorded at various potential scan rates from

10 to 200 mV s^{-1} (every 10 mV s^{-1}) for the same PANI deposits as in (A); corresponding variations of anodic peak currents with potential scan rates are shown in the insets.

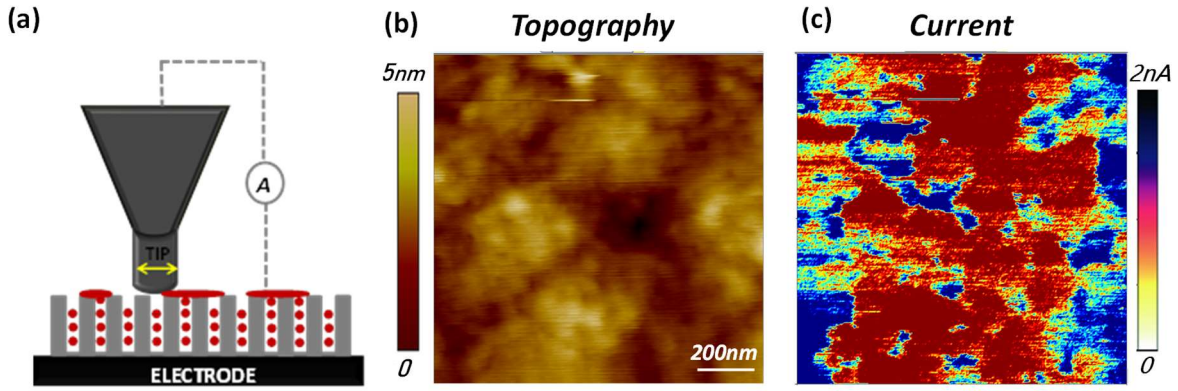

Figure 3. (a) C-AFM probe on top of the PANI@SiO_2 film. Red dots represent PANI filled inside the SiO_2 pores. Concurrently obtained resiscope C-AFM images of typical topography (b), and current (c) from the PANI-filled porous films. Scan area: 1 × 1 µm. In the current image, a bias voltage of -2V is applied.

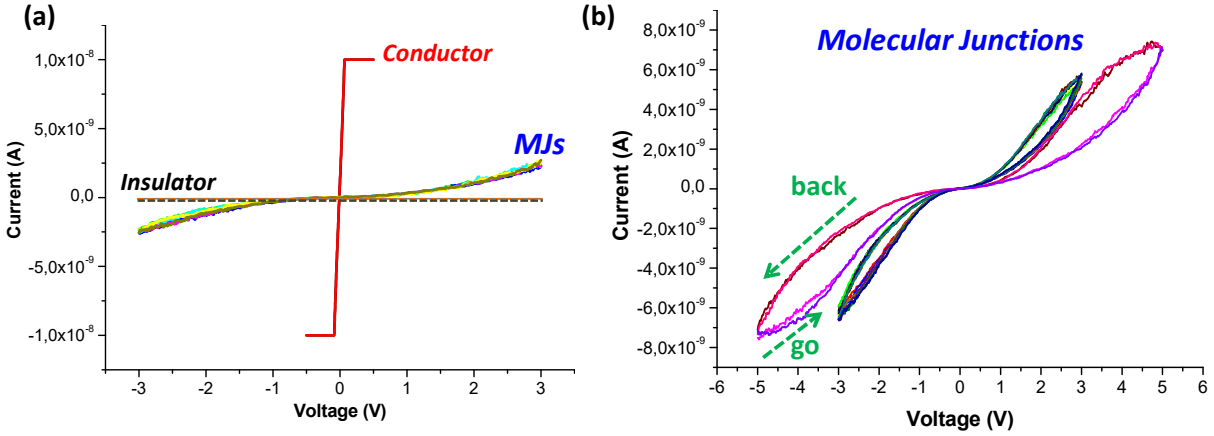

Figure 4. Typical C-AFM I/V curves of PANI@SiO_2 film: (a) combined I/V curves showing three different conductive behaviours (conductor, insulator and MJs). (b) Series of zoomed MJs I/V curves with hysteresis. Sweep voltage ranges from -3 to 3 V or from -5 to 5 V.